Supporting Information

Mo-cation/O-anion doping strategy for creating vacancy defects and cation multivalency to enhance the hydrogen evolution of ZnS under visible light

Xinru Wu[1,#], Tsz Lok Wan[2,#,*], Baoqian Yang[1], Dong-Hau Kuo[3,*], Pengkun Zhang[1], Minghao Liu[4], Samuel Ndaghiya Adawara[1], Dongfang Lu[1,*], Jinguo Lin[1,*], Xiaoyun Chen[1,*]

[1] College of Materials Engineering, Fujian Agriculture and Forestry University, Fuzhou 350002, China

[2] School of Mining and Petroleum Engineering, Department of Civil and Environmental Engineering, University of Alberta, Edmonton, AB, T6G 1H9, Canada

[3] Department of Materials Science and Engineering, National Taiwan University of Science and Technology, Taipei 106335, Taiwan

[4] School of Mechanical, Medical and Process Engineering, Queensland University of Technology, Brisbane, QLD, AU 4000, Australia

# These authors contributed equally to this work.

* Corresponding author

E-mail address: dhkuo@mail.ntust.edu.tw (D. H. Kuo)

E-mail address: twan1@ualberta.ca (T.L. Wan)

E-mail address: fjldf@126.com (D. Lu)

E-mail address: fjlinjg@126.com (J. Lin)

E-mail address: fjchenxy@126.com (X. Chen)

CONTENTS

1. Experimental Section

1.1 Apparent quantum efficiency computation

According to the literature reports for measuring the apparent quantum efficiency (AQE) [1, 2]. The experiment was measured under the photocatalytic reaction conditions of monochromatic light of 420 nm (λ), average radiation intensity (I) of 3.52 mW/cm^2, and irradiation area (A) of 32.75 cm^2. The total H_2 evolution with 50 mg of ZnMoOS-3 catalyst was 812.59 μmol, which can be used to determine the reacted photons (N_{reac}). The number of photons (N_{in}) illuminated to the reactor is computed according to the following equations:

$$N_{in} = \frac{\mathrm{E} \times \lambda}{h \times c} = \frac{\mathrm{A} \times \mathrm{I} \times \mathrm{t} \times \lambda}{h \times c} = \frac{32.75 \times 3.25 \times 10^{-3} \times 3600 \times 6 \times 420 \times 10^{-9}}{6.626 \times 10^{-34} \times 3 \times 10^{8}} = 5.26 \times 10^{21}$$

$$\mathrm{AQE} = \frac{N_{reac}}{N_{in}} \times 100\% = \frac{2 \times 6.02 \times 10^{23} \times 812.59 \times 10^{-6}}{5.26 \times 10^{21}} \times 100\% = 18.6\%$$

1.2 Electrochemical measurements

The electrochemical performance of the ZnMoOS catalyst was evaluated at room temperature using a three-electrode system and an electrochemical workstation. The catalyst, acetylene black, and polytetrafluoroethylene were uniformly coated on a titanium mesh (1 cm × 1 cm) in a mass ratio of 8: 1: 1. The working electrode was prepared by drying the coated sample in an oven at 85 ^{o}C for 4 hours. Cyclic voltammetry was used to assess the voltage stability of the catalyst using a 1.0 M KCl and 5 mmol/L Fe^{2+}/Fe^{3+} electrolyte solution. Mott-Schottky (MS), electrochemical impedance spectroscopy (EIS), transient photocurrent (TPC), linear sweep voltammetry (LSV), and cyclic voltammetry (CV) were performed in a 1 M Na_2SO_4 solution at a pH value of 6.8.

1.3 Details of computational models and parameters

All spin-polarized calculations were performed using first-principles calculations within the framework of density functional theory (DFT), as implemented in the Vienna Ab initio Simulation Package (VASP) [3, 4]. The interaction between valence and core electrons was described using the frozen-core projector augmented wave (PAW) method and the generalized gradient approximation (GGA) [4, 5]. The kinetic energy cutoff was set to 500 eV. Brillouin zone sampling was carried out using the Monkhorst-Pack scheme, with grids of 3×3×1 for structural optimization, 5×5×1 for self-consistent calculations, and 7×7×1 for charge density difference calculations. Long-range van der Waals (vdW) interactions were included using the DFT-D3 dispersion correction. The ZnOS and ZnMoOS-3 models were constructed as 3×3×1 supercells. Additionally, dipole correction was applied during all calculations.

The hydrogen evolution reaction (PHER) involves the adsorption of a proton on the catalyst surface, followed by molecular hydrogen generation via desorption. Using the computational hydrogen electrode (CHE) method, the adsorption energy of hydrogen (H^*) is calculated as:

$$\Delta E_* = E_{H*} - E_* - \frac{1}{2}E_{H_2} \quad (1)$$

where E_{H*} is the total energy of the studied catalyst with one adsorbed H atom. E_* and E_{H_2} is the energy of the catalyst and H_2 in the gas phase, respectively. The Gibbs free energy change (ΔG_{H*}) can be calculated by [6]

$$\Delta G_{H*} = \Delta E_{H*} + \Delta E_{ZPE} - T\Delta S_{H*} \quad (2)$$

where ΔE_{ZPE} denotes the zero-point energy change of the adsorbed H atom on the catalyst surface, which is calculated to be 0.04 eV [6]. Furthermore, ΔS_{H*} is the entropy change of H^* intermediate, which is estimated to be a constant value of -0.20 eV at 300 K [6]. This means that

$$\Delta G_{H*} = \Delta E_{H*} + 0.24\ eV \quad (3)$$

In addition, the electron transfer of the model is intuitively evaluated by the charge density difference (CDD), which is defined as following equation:

$$\rho = \rho_T - \rho_{catalyst} - \rho_H \quad (4)$$

where ρ_T, $\rho_{catalyst}$, and ρ_H are the electron of the H state adsorbed on the ZnOS or ZnMoOS-3, free ZnOS or ZnMoOS-3, and isolated H atom, respectively.

2. Additional Figures

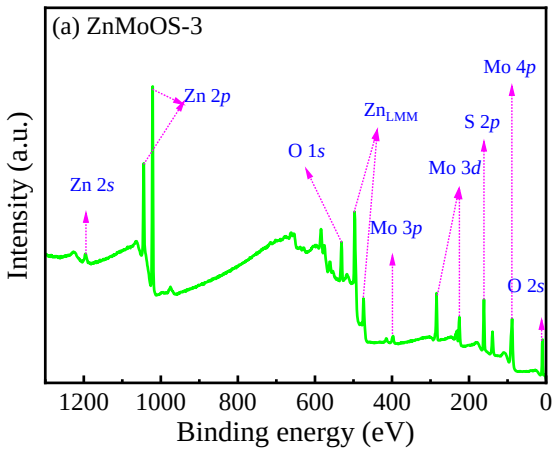

Fig. S1 The survey XPS spectrum of ZnMoOS-3

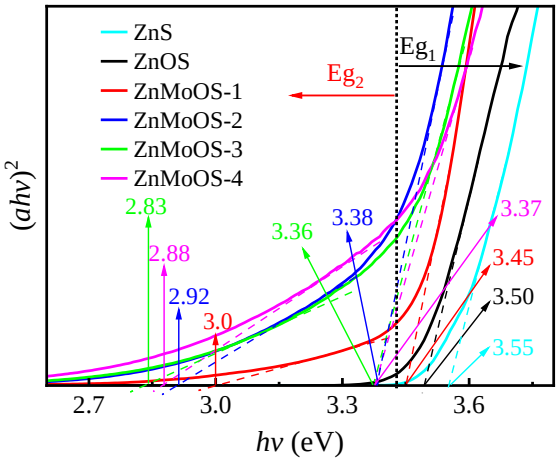

Fig. S2 (a) $(ahv)^2$ versus hv curves of ZnMoOS, ZnOS, and ZnS.

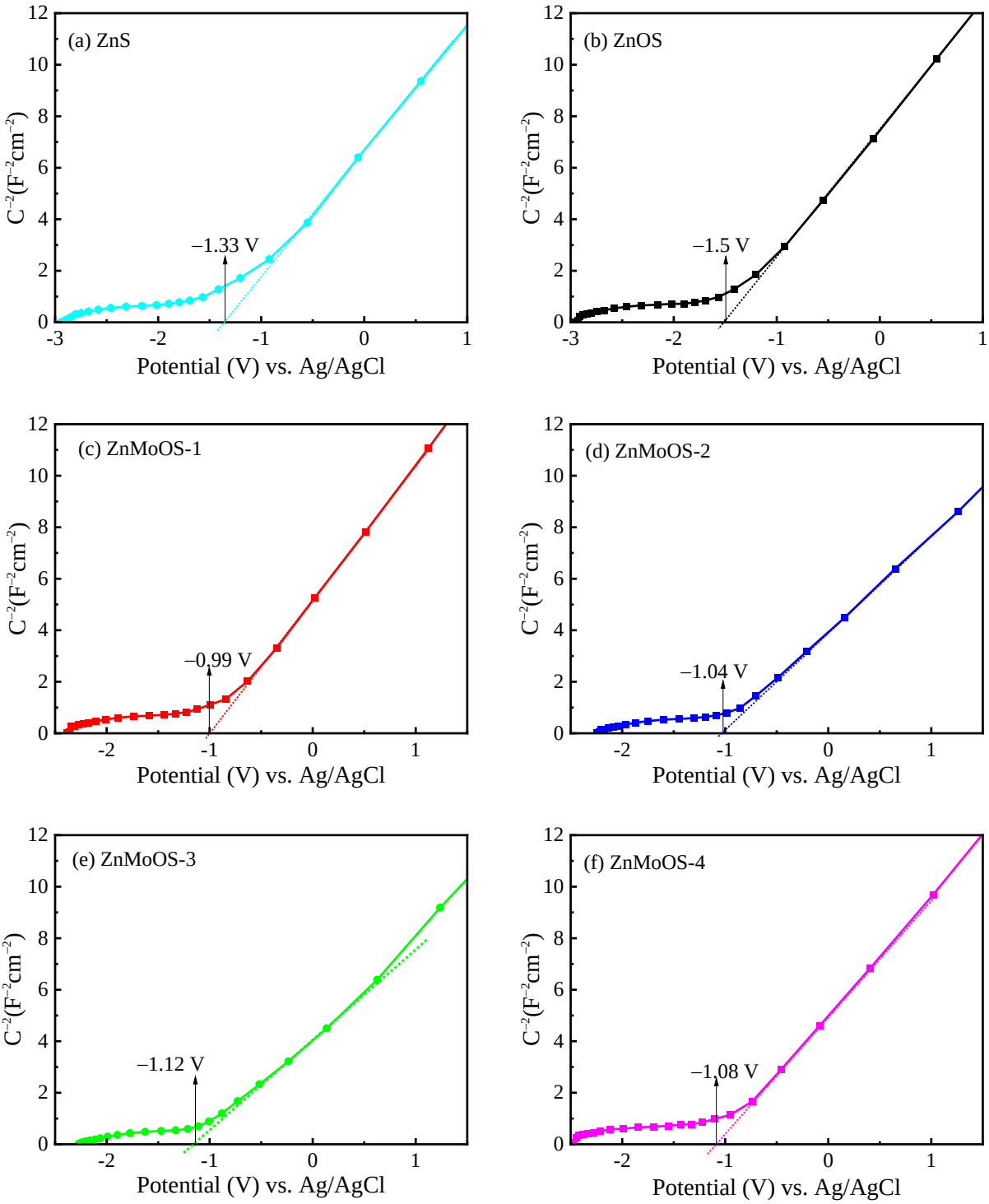

Fig. S3 Mott-Schottky curves of ZnS, ZnOS, ZnMoOS-1, ZnMoOS-2, ZnMoOS-3, and ZnMoOS-4 at 1000 kHz.

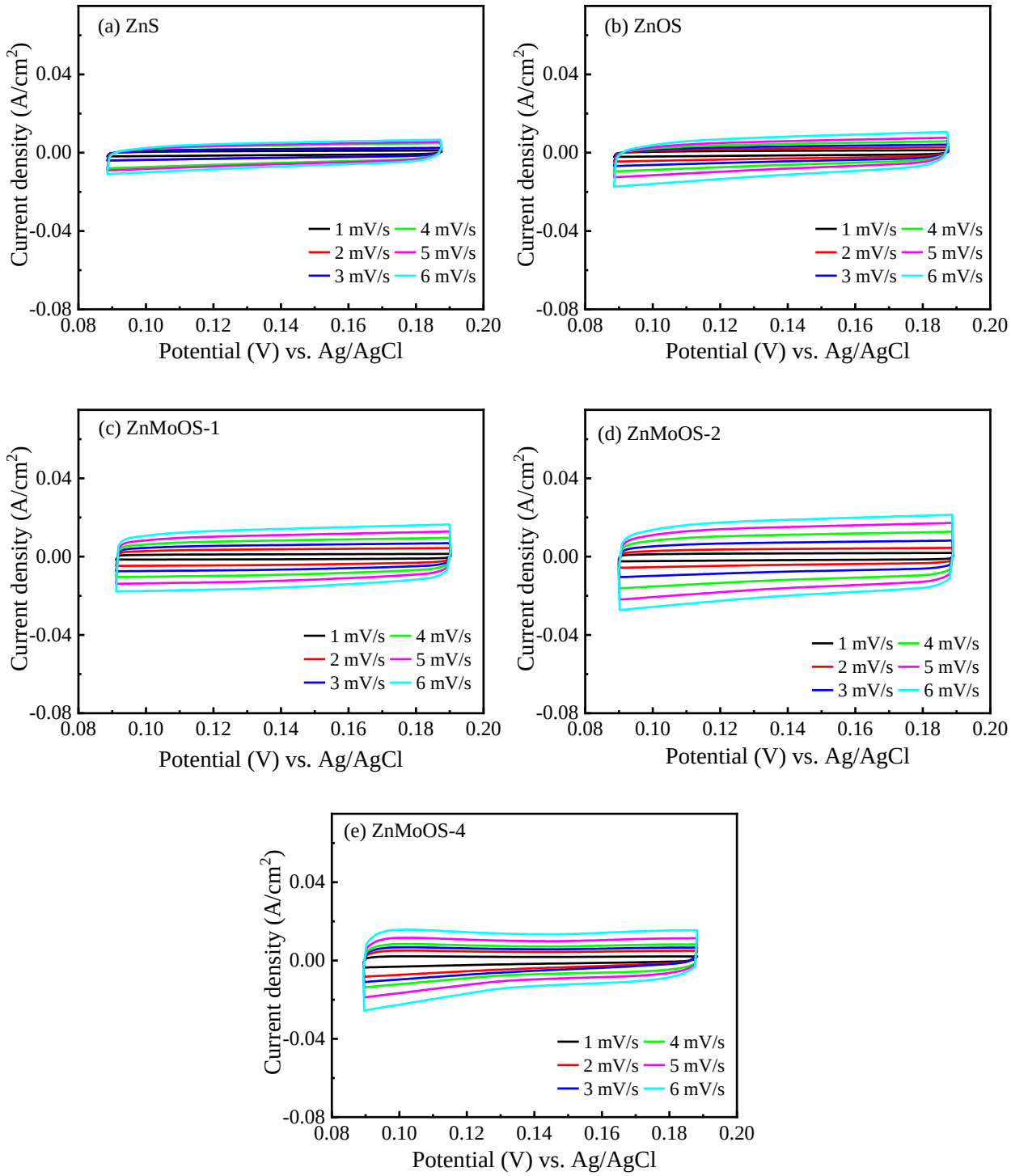

Fig. S4 Current density-potential plots of (a) ZnS, (b) ZnOS, (c) ZnMoOS-1, (d) ZnMoOS-2, and (e) ZnMoOS-4.

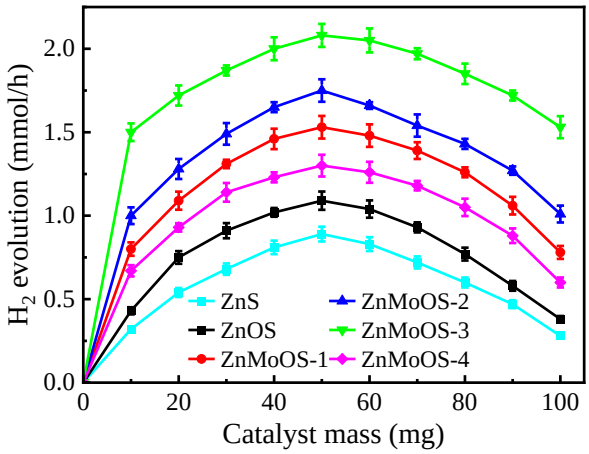

Fig. S5 Variation of PHER rate with the ZnMoOS, ZnOS, and ZnS amount.

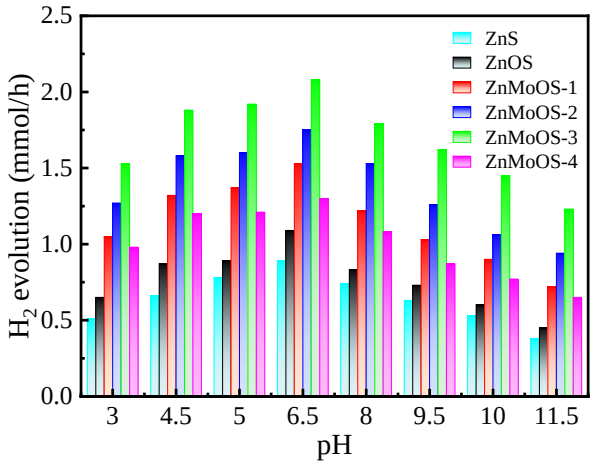

Fig. S6 PHER of ZnMoOS, ZnOS, and ZnS at different pH values.

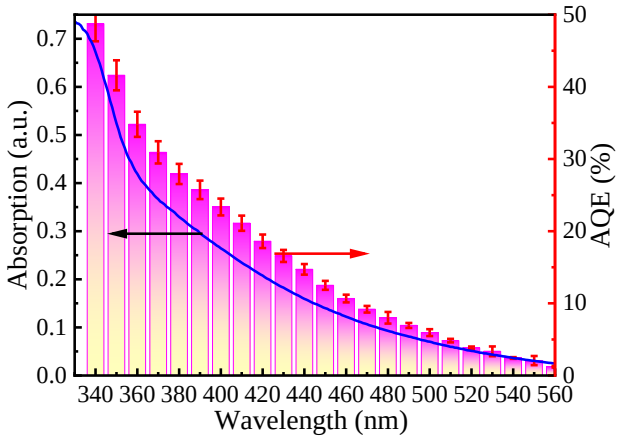

Fig. S7 Dependence of AQE ZnMoOS-3 as a function of irradiation wavelength, combining the UV−vis absorption spectrum.

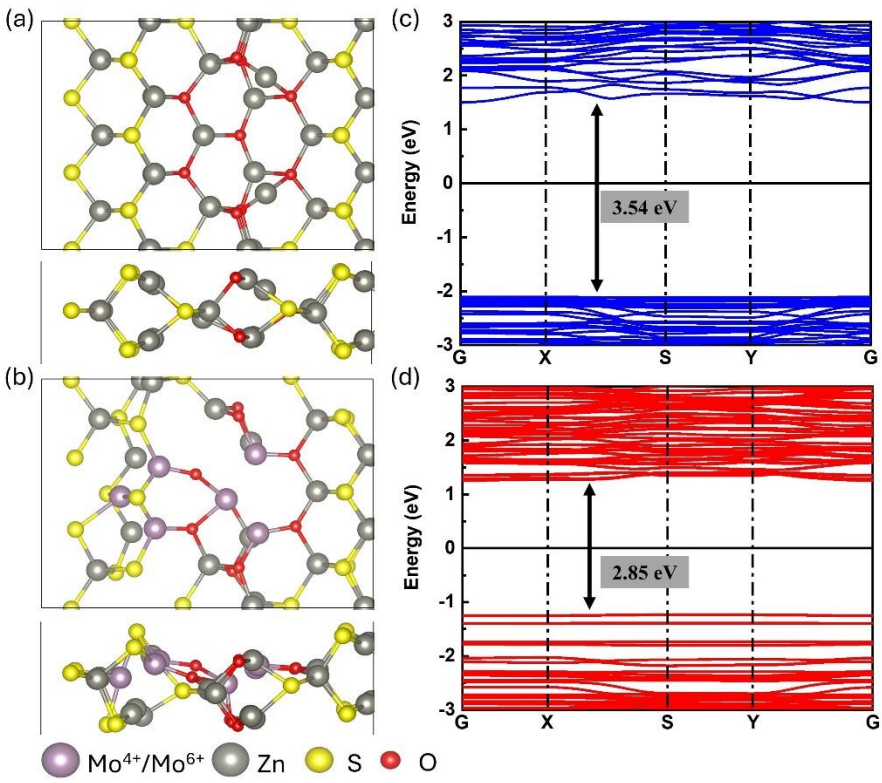

Fig. S8 Top views and side views of the (a) ZnOS and (b) ZnMoOS-3. Band structures for (c) ZnOS, and (d) ZnMoOS-3

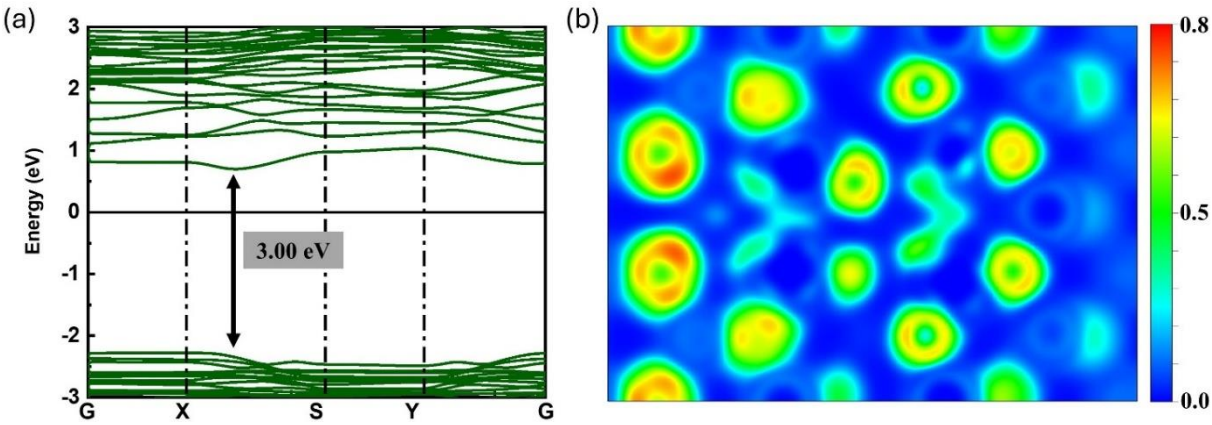

Fig. S9 (a) Band structures and (b) ELF for ZnMoOS-1.

3. Additional Tables

Table S1 Crystallinity, crystallite size, S_{BET}, and XPS analyses of ZnOS and ZnMoOS catalysts

Catalyst	Elements percentage (%)				Mo^{4+}/ Mo^{4+}+ Mo^{6+} (%)	Crystallinity (%)	Crystal size (nm)	S_{BET} (m^2/g)
	Zn	Mo	O	S				
ZnS	44.23	--	10.02	45.75	--	80.25	1.8	29.6
ZnOS	42.88	--	16.17	40.95	--	75.43	2.2	35.9
ZnMoOS-1	41.27	8.68	11.42	38.63	15.68	62.30	2.8	45.6
ZnMoOS-2	41.36	8.75	11.59	38.30	24.22	55.24	2.9	52.3
ZnMoOS-3	41.40	8.95	12.11	37.54	25.00	49.61	4.0	64.7
ZnMoOS-4	41.41	8.78	12.36	37.45	26.88	47.79	3.3	54.0
ZnMoOS-3 after reaction	41.36	8.92	12.58	37.14	24.98	48.99	3.8	64.2

Table S2 Elemental analyses tested by XRF

Catalyst	Zn (%)	Mo (%)	O (%)	S (%)
ZnS	44.34	--	10.08	45.58
ZnOS	42.84	--	16.18	40.98
ZnMoOS-1	41.25	8.67	11.44	38.64
ZnMoOS-2	41.34	8.74	11.60	38.32
ZnMoOS-3	41.41	8.97	12.12	37.50
ZnMoOS-4	41.43	8.79	12.34	37.44
ZnMoOS-3 after reaction	41.38	8.93	12.56	37.13

Table S3 Elemental analyses tested by SEM-EDS

Catalyst	Zn (%)	Mo (%)	O (%)	S (%)
ZnS	44.25	--	10.11	45.64
ZnOS	42.85	--	16.17	40.98
ZnMoOS-1	41.26	8.68	11.43	38.63
ZnMoOS-2	41.35	8.76	11.58	38.31
ZnMoOS-3	41.41	8.98	12.10	37.51
ZnMoOS-4	41.45	8.81	12.32	37.42
ZnMoOS-3 after reaction	41.39	8.94	12.56	37.11

Table S4 Average charge carrier lifetime of ZnMoOS and ZnOS

Catalyst	A_1	τ_1 (ns)	A_2	τ_2 (ns)	R^2	τ_{avg} (ns)
ZnS	1935.21	1.22	0.54	6.82	0.9945	1.216
ZnOS	822.23	1.27	4.15	4.05	0.9898	1.314
ZnMoOS-1	124.86	1.75	2.38	5.14	0.9974	1.930
ZnMoOS-2	62.17	1.88	3.09	5.51	0.9986	2.342
ZnMoOS-3	8.80	3.29	2.14	6.31	0.9992	4.250
ZnMoOS-4	251.71	1.48	3.73	4.94	0.9985	1.643

Table S5 Reports on PHER performance over ZnS-based catalysts under visible light

Catalyst	Sacrificial agent	Light source	AQE/AQY (%)	PHER rate (mmol/g/h)	Refs.
Mo-Sv-ZIS	Na_2S/Na_2SO_3	300 W Xe	AQY 21.24 (420 nm)	5.739	[7]
MoS_2/O-$ZnIn_2S_4$	Na_2S/Na_2SO_3	300 W Xe	AQY 2.53 (420 nm)	4.002	[8]
CdS/Ni-Mo-S	10 vol% $C_6H_{15}NO_3$	300 W Xe	N/A	0.838	[9]
Mo/S/g-C_3N_4	10 vol% CH_3OH	300 W Xe	N/A	0.294	[10]
Zn-Cd-Mo-S	Na_2S/Na_2SO_3	300 W Xe	AQE 6.9 (420 nm)	23.32	[11]
Mo/S-In_2S_3	10 vol% $C_6H_{15}NO_3$	300 W Xe	AQE 10.23 (420 nm)	5.45	[12]
$CdIn_2S_4$@MoS_2	10 vol% $C_6H_{15}NO_3$	300 W Xe	N/A	0.539	[13]
ZnO@ZnS	Na_2S/Na_2SO_3	300 W Xe	AQE 2.58 (420 nm)	2.4	[14]
ZnO/ZnS/CdS	Na_2S/Na_2SO_3	300 W Xe	N/A	2.64	[15]
ZnS/TiO_2	Na_2S/Na_2SO_3	300 W Xe	N/A	1.718	[16]
CdS/MoS_2/ZnS	Na_2S/Na_2SO_3	300 W Xe	AQY 8.55 (420 nm)	11.902	[17]
ZnS/ZnAl-LDH	50 vol% CH_3OH	300 W Xe	N/A	4.41	[18]
$ZnIn_2S_4$/ZnS	Na_2S/Na_2SO_3	300 W Xe	N/A	8.5	[19]
ZnO@ZnS@FeOOH	10 vol% CH_3OH	300 W Xe	N/A	0.53	[20]
$CdIn_2S_4$/ZnS	Na_2S/Na_2SO_3	300 W Xe	AQE 2.15 (365 nm)	3.74	[21]
$CdIn_2S_4$/ZnS	Na_2S/Na_2SO_3	300 W Xe	N/A	10.80	[22]
ZnS/NiS	Lactic acid	300 W Xe	AQE 30.4 (420 nm)	10.64	[23]
Ni_2P/ZnS/g-C_3N_4	Na_2S/Na_2SO_3	250 W Xe	N/A	3.991	[24]
ZnO/ZnS/Co_3O_4	10 vol% CH_3OH	300 W Xe	N/A	0.153	[25]
$NiCo_2O_4$@ZnS	Na_2S/Na_2SO_3/NaCl	300 W Xe	N/A	0.88	[26]
Fe_3O_4@ZnS	Na_2S/Na_2SO_3/NaCl	300 W Xe	N/A	3.9	[27]
$Zn_xCd_{1-x}S$/ZnS	Lactic acid	300 W Xe	AQE 10 (420 nm)	16.7	[27]
Zn-$AgIn_5S_8$/ZnS	Na_2S/Na_2SO_3	300 W Xe	N/A	0.892	[28]
Cu_2O/CuS/ZnS	Na_2S/Na_2SO_3	5 W LED	N/A	1.109	[29]
ZnMoOS-3	Na_2S/Na_2SO_3	300 W Xe	AQE 18.6 (420 nm)	41.6	This work

References:

[1] C. Li, T. Zhou, M. Yan, S. Cheng, Y. Wang, J. Sun, G. Chen, H. Dong, Intramolecular π-conjugated channel expansion achieved by doping cross-linked dopants into carbon nitride frameworks for propelling photocatalytic hydrogen evolution and mechanism insight, *Inorg. Chem. Front.*, 9 (2022) 60-69.

[2] M. Dan, S. Wei, D.E. Doronkin, Y. Li, Z. Zhao, S. Yu, J.-D. Grunwaldt, Y. Lin, Y. Zhou, Novel MnS/$(In_xCu_{1-x})_2S_3$ composite for robust solar hydrogen sulphide splitting via the synergy of solid solution and heterojunction, *Appl. Catal. B-Environ.*, 243 (2019) 790-800.

[3] G. Kresse, J. Furthmüller, Efficiency of ab-initio total energy calculations for metals and semiconductors using a plane-wave basis set. *Comput. Mater. Sci.*, 6 (1996) 15-50.

[4] G. Kresse, J. Furthmüller, Efficient iterative schemes for ab initio total-energy calculations using a plane-wave basis set. *Phys. Rev. B*, 54 (1996) 11169.

[5] J.P. Perdew, K. Burke, M. Ernzerhof, Generalized gradient approximation made simple. *Phys. Rev. Lett.*, 77 (1996) 3865.

[6] J.K. Nørskov, T. Bligaard, A. Logadottir, J. Kitchin, J.G. Chen, S. Pandelov, U. Stimming, Trends in the exchange current for hydrogen evolution. *J. Electrochem. Soc.*, 152 (2005) J23.

[7] W. Guan, L. Zhang, P. Wang, Y. Wang, H. Wang, X. Dong, M. Meng, L. Sui, Z. Gan, L. Dong, L. Yu, Highly efficient photocatalytic hydrogen evolution over Mo-doped $ZnIn_2S_4$ with sulfur vacancies, *Nanomaterials-Basel.*, 12 (2022) 3980.

[8] Y. Peng, X. Guo, S. Xu, Y. Guo, D. Zhang, M. Wang, G. Wei, X. Yang, Z. Li, Y. Zhang, F. Tian, Surface modulation of MoS_2/O-$ZnIn_2S_4$ to boost photocatalytic H_2 evolution, *J. Energy Chem.*, 75 (2022) 276-284.

[9] H. Li, J. Pan, W. Zhao, C. Li, The 2D nickel□molybdenum bimetals sulfide synergistic modified hollow cubic CdS towards enhanced photocatalytic water splitting hydrogen production, *Appl. Surf. Sci.*, 497 (2019) 143769.

[10] Y. Li, S. Zhu, Y. Liang, Z. Li, S. Wu, C. Chang, S. Luo, Z. Cui, One-step synthesis of Mo and S co-doped porous g-C_3N_4 nanosheets for efficient visible-light photocatalytic hydrogen evolution, *Appl. Surf. Sci.*, 536 (2021) 147743.

[11] P. Guo, D. Zhang, X. Liu, W. Liu, R. Wang, Z. Zhang, S. Qiu, In situ self-assembly of mesoporous Zn-Cd-Mo-S quaternary metal sulfides with double heterojunction synergistic charge transfer for boosting photocatalytic hydrogen production, *J. Alloy. Compd.*, 921 (2022) 166066.

[12] M. Han, L. Liu, B. Guo, Z. Zhang, X. Li, Y. Chang, S. Luo, W. Lu, S. Li, J. Ye, Bi&Mo co-doped In_2S_3 nano-foam blocks for boosted photocatalytic hydrogen generation, *Int. J. Hydrogen Energ.*, 78 (2024) 140-147.

[13] Y. Lu, H. Liu, L. Wang, Y. Geng, M. Zhang, Preparation of $CdIn_2S_4$ nanoparticles@MoS_2 microrods heterojunctions for boosted photocatalytic hydrogen production, *J. Alloy. Compd.*, 982 (2024) 173750.

[14] H. Ren, K. Ye, H. Chen, F. Wang, Y. Hu, Q. Shi, H. Yu, R. Lv, M. Chen, ZnO@ZnS core-shell nanorods with homologous heterogeneous interface to enhance photocatalytic hydrogen production, *Colloid. Surface. A.*, 652 (2022) 129844.

[15] K. He, ZnO/ZnS/CdS three-phase composite photocatalyst with a flower cluster structure: Research on its preparation and photocatalytic activity hydrogen production, *Int. J. Hydrogen Energ.*, 51 (2024) 30-40.

[16] X. Gui, Y. Zhou, Q. Liang, M. Zhou, X. Li, S. Xu, Z. Li, Construction of porous ZnS/TiO_2 S-scheme heterostructure derived from MOF-on-MOF with boosting photocatalytic H_2-generation

activity, *Int. J. Hydrogen Energ.*, 48 (2023) 38237-38250.

[17] H. Yang, B. Hu, H. Sun, G. Ma, S. Wang, Y. Li, H. Zhang, H. Xie, H. Quan, H. Zhang, Stepped fluorinated CdS/MoS_2/ZnS nanoparticles constructed on a multifunctional platform with Zn(OH)F nanoflowers for highly active photocatalytic H_2 production, *Sep. Purif. Technol.*, 347 (2024) 127461.

[18] D. Téllez-Flores, M. Sánchez-Cantú, F. Tzompantzi, A.G. Romero-Villegas, C. Tzompantzi-Flores, J.E. Carrera-Crespo, R. Pérez-Hernández, E. Rubio- Rosas, Influence of the Zn/Al molar ratio over the photocatalytic hydrogen production by ZnS/ZnAl-LDH composites, *Int. J. Hydrogen Energ.*, (2024) 0360-3199.

[19] M. Li, S. Li, Y. Li, P. He, Y. Xiao, J. Chen, T. Ren, Decorating ZnS by $ZnIn_2S_4$ to fabricate hybrid photocatalyst $ZnIn_2S_4$/ZnS for high photocatalytic hydrogen generation performance, *Mater. Lett.*, 334 (2023) 133757.

[20] T. Chigan, B. Ma, C. Zhang, X. Li, D. Jia, H. Li, P. Yang, Coupling interface constructions of ZnO@ZnS@FeOOH for photocatalytic hydrogen production performance, *Colloid. Surface. A.*, 688 (2024) 133551.

[21] L. Xie, G. Liu, R. Suo, Z. Xie, H. Liu, J. Chen, J. Chen, C. Lu, Construction of a Z-scheme $CdIn_2S_4$/ZnS heterojunction for the enhanced photocatalytic hydrogen evolution, *J. Alloy. Compd.*, 948 (2023) 169692.

[22] M. Li, T. Ren, Y. Li, S. Li, P. He, Y. Xiao, J. Chen, Constructing $CdIn_2S_4$/ZnS type-I band alignment heterojunctions by decorating $CdIn_2S_4$ on ZnS microspheres for efficient photocatalytic H_2 evolution, *Int. J. Hydrogen Energ.*, 48 (2023) 37224-37233.

[23] Y. Li, X. Liu, Y. Wang, Y. Liu, R. Liu, H. Mu, Y. Hao, X. Wang, F. Li, Constructing interfacial electric field and Zn vacancy modulated ohmic junctions ZnS/NiS for photocatalytic H_2 evolution,

Green Energy Environ., (2024) 2468-0257.

[24] R. Rameshbabu, J.K.S. Paw, K. Ajaijawahar, V. Vinoth, S. Jadoun, N. Pugazhenthiran, T.S. Kiong, Fabricating of multi-interfacial charge transfer paths in the novel noble-metal-free Ni_2P/ZnS/g-C_3N_4 ternary nanocomposite for enhanced charge separation and transfer for photocatalytic H_2 generation, *J. Alloy. Compd.*, 997 (2024) 174830.

[25] F. Ma, X. Xu, C. Huo, C. Sun, Q. Li, Z. Yin, S. Cao, Dual heterogeneous structures promote electrochemical properties and photocatalytic hydrogen evolution for inverse opal ZnO/ZnS/Co_3O_4 crystals, *Inorg. Chem.*, 63 (2024) 8782-8790.

[26] C. Chang, Z. Lee, M. Wei, C. Chang, K. Chu, Photocatalytic hydrogen production by magnetically separable Fe_3O_4@ZnS and $NiCo_2O_4$@ZnS core-shell nanoparticles, *Int. J. Hydrogen Energ.*, 40 (2015) 11436-11443.

[27] J. Dong, W. Fang, W. Xia, Q. Lu, X. Zeng, Facile preparation of $Zn_xCd_{1-x}S$/ZnS heterostructures with enhanced photocatalytic hydrogen evolution under visible light, *RSC Adv.*, 11 (2021) 21642-21650.

[28] Y. Liu, X. Wang, G. Gong, A.U. Khan, G. Li, T. Ren, Q. Chen, L. Li, B. Mao, Ultrathin-shelled Zn-$AgIn_5S_8$/ZnS quantum dots with partially passivated trap states for efficient hydrogen production, *Catalysts*, 14 (2024) 298.

[29] Y.C. Chang, Y.C. Chiao, Y.X. Fun. Cu_2O/CuS/ZnS nanocomposite boosts blue LED-light-driven photocatalytic hydrogen evolution, *Catalysts*, 12 (2022) 1035.